Geophysical Research Letters

RESEARCH LETTER
10.1029/2023GL103324

Key Points:

- The energy budget in magnetic reconnection is not significantly affected by cold ion beams for constant inflow plasma global parameters
- The hotter ion population gains more energy during magnetic reconnection than the colder one
- Most of the energy gain of hot ions is in the form of internal energy, while the energy transferred to the cold ions is more balanced

Correspondence to:
J. Dargent,
jeremy.dargent@ruhr-uni-bochum.de

Citation:
Dargent, J., Toledo-Redondo, S., Divin, A., & Innocenti, M. E. (2023). Energy conversion by magnetic reconnection in multiple ion temperature plasmas. *Geophysical Research Letters*, *50*, e2023GL103324. https://doi.org/10.1029/2023GL103324

Received 16 FEB 2023
Accepted 12 MAY 2023

Author Contributions:
Conceptualization: J. Dargent
Data curation: J. Dargent
Formal analysis: J. Dargent
Funding acquisition: M. E. Innocenti
Methodology: J. Dargent
Resources: M. E. Innocenti
Writing – original draft: J. Dargent

Energy Conversion by Magnetic Reconnection in Multiple Ion Temperature Plasmas

J. Dargent[1], S. Toledo-Redondo[2], A. Divin[3], and M. E. Innocenti[1]

[1]Institut für Theoretische Physik, Ruhr-Universität Bochum, Bochum, Germany, [2]Department of Electromagnetism and Electronics, University of Murcia, Murcia, Spain, [3]Department of Earth's Physics, St. Petersburg State University, St. Petersburg, Russia

Abstract Magnetic reconnection is a process that converts magnetic energy into kinetic energy, both bulk and thermal. We study the energy partition in magnetotail reconnection in the presence of cold ion populations of ionospheric origin using kinetic simulations. We compare two simulations with one or two ion populations, but same ion moments. The ion distribution in the simulation with cold ions therefore corresponds to a non-Maxwellian distribution with a large tail. The global energy budget does not change in the two cases, but when focusing on sub-populations, the hot ion population (i.e., the tail of the velocity distribution function) gains more energy than the cold ion population (i.e., the core of the distribution). Hot and cold ions also gain different percentages of bulk and thermal energy.

Plain Language Summary Magnetic reconnection is a process that converts magnetic energy into acceleration (bulk kinetic energy) and heating (thermal kinetic energy). In the magnetosphere, we often see a cold plasma population of ionospheric origin, on top of the hot magnetospheric plasma. We study the energy partition in magnetotail reconnection in the presence of those cold ions using simulations. We compare two simulations with and without cold ions, but same global parameters. We observe that the total energy partition is not significantly different between the simulations. But when focusing on the cold ion simulation, we see that hot ions gains more energy than cold ions and also have a larger bulk over thermal energy gain.

1. Introduction

The question of conversion of energy from fields to particles is one of the main problems of space and astrophysical plasmas. At the core of this issue is magnetic reconnection, that converts magnetic energy into thermal energy and bulk kinetic energy by altering magnetic field topology. The change in magnetic topology also efficiently mixes plasmas from different origins. It plays a major role in many eruptive processes in space plasmas, such as coronal mass ejections (Gosling et al., 1995), solar flares (Shibata et al., 1995), or geomagnetic substorms (Angelopoulos et al., 2008). Several studies have focused on understanding which percentage of the available magnetic energy is transferred to the different particle populations, for example, electrons and ions, as a function of plasma parameters (Haggerty et al., 2015; Yamada et al., 2014). Furthermore, one can investigate in *which form* of particle energy is magnetic energy converted. Using ManetoHydroDynamics and small-scale Particle-In-Cell (PIC) simulations, Birn and Hesse (2005, 2010) have showed that most of energy released in magnetic reconnection is converted into thermal energy, using kinetic energy as a mediator. Using hybrid PIC simulations, Aunai et al. (2011) shows that most of the energy transfer is converted into ion thermal energy, mainly through the enthalpy flux. Eastwood et al. (2013) confirmed with spacecraft observations that the ion enthalpy flux is dominant in the partition of energy flux. More recently, Shu et al. (2021) confirmed those results using a larger-scale full PIC simulation.

Numerical energy studies until now have focused on energy partition in the presence of a single ion (and sometimes electron) population. This doesn't take into account one of the most characteristic features of collisionless plasma: without thermalization via collisions, multiple ion populations can co-exist and distribution functions are not necessarily Maxwellian. Such a situation is relatively common. For example, we find several electron populations in the solar wind (Pilipp et al., 1987), that can scatter into one another only through collisionless processes (Micera et al., 2021), or ions of ionospheric origin in the Earth's magnetosphere (Toledo-Redondo et al., 2021). Since the presence of multiple populations is such a common occurrence, it is of extreme relevance to understand how the presence of multiple populations of the same species affects energy partition. In addressing this

open problem, we select the Earth's magnetosphere as our case study: the presence of multiple ion population is attested and has already been the subject of many studies, thanks to the large amount of data available (André & Cully, 2012; Dandouras, 2013; Fuselier et al., 2016; Toledo-Redondo et al., 2021). Many works have investigated ionospheric ions impact on magnetic reconnection and its reconnection rate (Dargent et al., 2017, 2020; Divin et al., 2016; Spinnangr et al., 2021). However, this study is the first to address the impact of multiple population on magnetic reconnection energy partition.

In this study, we specifically look at the impact of the ion distribution function on the energy budget of magnetic reconnection. We perform two simulations of symmetric magnetic reconnection with the same global macroscopic parameters (electromagnetic fields, density, temperature, etc.), but different microscopic ones (shape of the ion distribution functions). In the first simulation ions are loaded with a single Maxwellian distribution, while in the second one, ions are loaded as a double Maxwellian distributions, therefore simulating a case with two plasma populations. The first configuration corresponds to the default description of space plasma used in most theoretical and numerical studies (Aunai et al., 2011; Birn & Hesse, 2005, 2010; Shu et al., 2021), while the second one describes a typical reconnection where cold ions of ionospheric origin coexist with hotter magnetospheric ions. We first look at the difference between the two simulations, to see how the magnetic reconnection energy budget is affected by the microscopic configuration of the plasma. Then, we focus on the simulation with cold ions and compare the relative energy gain of each ion population: which population gains more energy and how is this energy partitioned?

2. Simulation Setup

In this paper, we present two two-dimensional (2D-3V) fully kinetic simulations of symmetric magnetic reconnection using the implicit PIC code ECsim (Gonzalez-Herrero et al., 2019). The use of a semi-implicit code reduces the constraint on the small scale resolution, thus reducing the cost of fully kinetic PIC simulations with respect to their explicit counterpart. One can then simulate larger domain, for longer times, or at a larger mass ratio. Both simulations share the same electric and magnetic field, total density, and temperature profiles. They only differ by the velocity distribution function of the ions.

All physical quantities are normalized using ion characteristic quantities. The magnetic field and density are normalized to B_0 (the asymptotic value of the magnetic field in the inflow regions) and n_0 (the peak density of the Harris sheet), respectively. The masses and charges are normalized to the proton mass m_p and charge e, time is normalized to the inverse of the proton gyrofrequency $\omega_{ci}^{-1} = m_p/eB_0$ and length to the proton inertial length $d_i = c/\omega_{pi}$, where c is the speed of light in vacuum and $\omega_{pi} = \sqrt{n_0 e^2/m_p \epsilon_0}$ is the proton plasma frequency. Velocities are normalized to the Alfvén velocity $v_{Al} = d_i\omega_{ci}$. Temperatures are normalized to $T_0 = B_0^2/(\mu_0 k_B n_0) = m_p v_{Al}^2/k_B$, with v_{Al} the Alfven velocity.

The initial configuration for both simulations is an Harris equilibrium with two current layers in the (x, y) plane with a half-width of $\lambda = 0.5d_i$ that are located at $y = L_y/4$ and $y = 3L_y/4$ in a rectangular computational domain of length $L_x = 300\, d_i$ and width $L_y = 150\, d_i$. The lower layer, on which we will focus from now on, is perturbed to trigger magnetic reconnection while the upper one is left unperturbed. The peak of the Harris current sheet density is equal to n_0 and on top of the current layer plasma, we add a uniform background plasma of density $n_b = 0.2n_0$. There are $n_x = 3{,}008$ cells in the x direction, $n_y = 1{,}536$ cells in the y direction and initially 225 ions per cell per ion population and 900 electrons per cell per electron population. The first simulation (simulation 1, without cold ions) has two ion populations (layer ions + background ions) and same for the electrons. The ion temperature is uniform and equal to $T_i = 0.4T_0$ for all ion populations, while the temperature ratio between ions and electrons is equal to $T_e/T_i = 0.2$. In the second simulation (simulation 2, with cold ions), the background ions are split in two populations (hot and cold ions) of equal density ($n_{ic} = n_{ih} = n_b/2$) and with a temperature ratio of $T_{ih}/T_{ic} = 500$. The average temperature of the background ions $T_i = (n_{ic}T_{ic} + n_{ih}T_{ih})/n_b$ remains the same as to the first simulation. The other populations are left unchanged. Particles of each population are loaded using local Maxwellian distributions. The time step is $dt = 0.002\ \ \omega_{ci}^{-1}$. The mass ratio m_i/m_e is 256. We fix $\omega_{pi}/\omega_{ci} = c/v_{Al} = 102.6$. The system has periodic boundary conditions in both directions. Energy in the simulations is well-conserved, with a total energy loss of ~3% at $T = 150\ \ \omega_{ci}^{-1}$.

3. Energy Budget Analysis

3.1. Methodology

In this study, we split the total energy into different contributions: the magnetic energy density $W_B = B^2/2\mu_0$, the electric energy density $W_E = \epsilon_0 E^2/2$, the bulk kinetic energy density of each population (subscript s, with s the

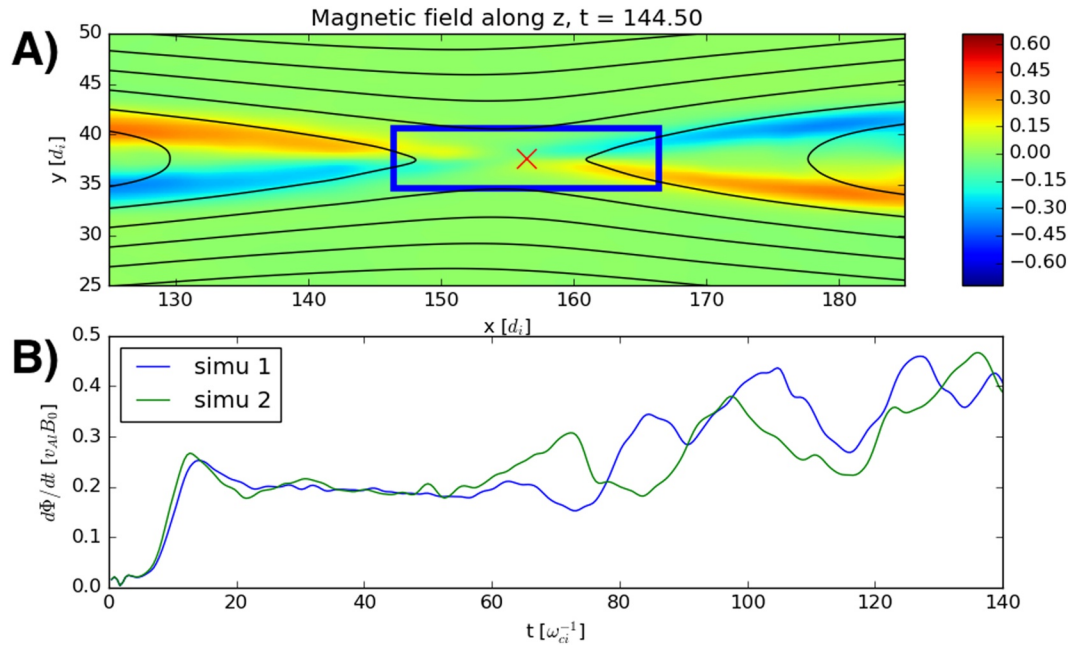

Figure 1. Panel (a) Out-of-plane magnetic field B_z from simulation 1. The blue box indicates the area $\mathcal{A}$ of interest for the energy budget. The black lines represent the in-plane projection of the magnetic field lines. The red cross gives the position of the X point. Panel (b) Reconnection rate of simulations 1 and 2. Reconnection rate is here calculated as the normalized time derivative of the magnetic flux Φ in the simulation plane (x, y) calculated at the X point.

population) $K_s \equiv 1/2 m_s n_s v_s^2$, and the thermal kinetic energy density of each population $u_s \equiv 1/2\ Tr(\mathbf{P}_s)$ (where $Tr(\mathbf{P}_s)$ is the trace of the full pressure tensor $\mathbf{P}_s$). Note however that in our area of interest $W_B \gg W_E$, so the electromagnetic energy can be approximated as the magnetic energy. The Eulerian evolution of these quantities is governed by the following equations:

$$\frac{\partial(W_B + W_E)}{\partial t} + \nabla \cdot \mathbf{\Pi} = S_m \tag{1}$$

$$\frac{\partial K_s}{\partial t} + \nabla \cdot (K_s \mathbf{v}_s) = S_{k_s} \tag{2}$$

$$\frac{\partial u_s}{\partial t} + \nabla \cdot (\mathbf{q}_s + \mathbf{H}_s) = S_{u_s} \tag{3}$$

where $\mathbf{\Pi} = \mathbf{E} \times \mathbf{B}/\mu_0$ is the Poynting flux, $\mathbf{q}_s$ the heat flux vector and $\mathbf{H}_s = u_s \mathbf{v}_s + \mathbf{P}_s \cdot \mathbf{v}_s$ the enthalpy flux. S_m, S_{k_s} and S_{u_s} are the energy source terms, which result from the transfers between the different forms of energies, and whose sum over all plasma species and magnetic energy equal to zero due to the total energy conservation. They are respectively equal to $S_m = -\mathbf{J} \cdot \mathbf{E}$ for the magnetic energy source term, $S_{k_s} = n_s q_s \mathbf{v}_s \cdot \mathbf{E} - (\nabla \cdot \mathbf{P}_s) \cdot \mathbf{v}_s$ for the bulk kinetic energy density source terms and $S_{u_s} = (\nabla \cdot \mathbf{P}_s) \cdot \mathbf{v}_s$ for the thermal kinetic energy density source terms. The energy source terms are located on the right-hand side of the equations, while on the left-hand side we have two components: the local time evolution of the energy density and the local divergence of this energy density flux.

In this study, we are interested in the conversion of magnetic energy into kinetic energy by magnetic reconnection. Given the importance of the demagnetization of electrons and ions in the onset of magnetic reconnection, we focus our work on the ion demagnetization region. We integrate the different terms of Equations 1–3 over an area centered on the reconnection X point and whose area $\mathcal{A}$ (depicted on Figure 1a) encompass the ion diffusion region. The area corresponds to a rectangle with side's size of $20 \times 6\ d_i$. Given that the area $\mathcal{A}$ size has to be constant while the size of the diffusion region is not, we arbitrarily fixed this area as the smaller rectangle encompassing the region of increased $\mathbf{J} \cdot \mathbf{E}$ centered on the X point and with corners matching as much as possible with the separatrices, for simulation 1 and $t = 144.5\ \omega_{ci}^{-1}$. Therefore, the upper and lower sides of this area roughly correspond to the inflow boundaries of the diffusion region, while the left and right sides are the outflow

boundary of the diffusion region. Note that to compare simulations, the area $\mathcal{A}$ is kept identical in simulation 2, despite a slightly larger hot ion diffusion region.

We integrate over the area $\mathcal{A}$ the different terms of Equations 1–3. From the source terms, we get the energy gains associated with each source:

$$E_m(t) = \int_{\mathcal{A}} S_m(x, y, t) dx dy \tag{4}$$

$$E_{k_s}(t) = \int_{\mathcal{A}} S_{k_s}(x, y, t) dx dy \tag{5}$$

$$E_{u_s}(t) = \int_{\mathcal{A}} S_{u_s}(x, y, t) dx dy \tag{6}$$

From the integration of the source terms, we get information on how the magnetic energy is distributed between the thermal and bulk kinetic energy of the different populations. In the steady state approximation, that is, $\partial/\partial t = 0$, those terms are equal to the integration over the whole contour C of the flux terms on the left-hand side of the Eulerian equations, that is, $E_i(t) = \phi_i^C(t)$ for $i \equiv m, k_s, u_s$ with:

$$\phi_m^C(t) = \int_C \Pi(x, y, t) \cdot \mathbf{dl} \tag{7}$$

$$\phi_{k_s}^C(t) = \int_C (K_s \mathbf{v}_s)(x, y, t) \cdot \mathbf{dl} \tag{8}$$

$$\phi_{u_s}^C(t) = \int_C (\mathbf{q}_s + \mathbf{H}_s)(x, y, t) \cdot \mathbf{dl} \tag{9}$$

The physical meaning of this equality is that the difference between the energy fluxes that enter and exit the area through the contour C is equal to the energy gain/loss of the corresponding energy source. In the case of our simulations, we never reach a steady state because of the motion of the X point along x (Dargent et al., 2016). Given that the area $\mathcal{A}$ position is linked to the X point position, the box itself is not static in the simulation frame. Therefore, to correct for this drift, all the values in the rest of the paper are calculated in the reference frame of the X point. The X point position is calculated by looking for the position of a saddle point in the magnetic flux. In case of several saddle points, the one with the smaller flux value is designed as the dominant X point.

3.2. Energy Partition in Simulations With and Without Cold Ions

In Figure 1b, we can see the comparison of the reconnection rates with time in both simulations. The reconnection rate is the normalized electric field along z (i.e., reconnection electric field) at the X point. However, we are using the time derivative of the magnetic flux in the simulation plane (x, y) $d\Phi/dt$ instead, which is identical to E_z for 2D simulations (Pritchett, 2008; Shay et al., 2001). We can see that the reconnection rate (Figure 1b) remains quasi unchanged between the simulations. This is consistent with previous works on cold ions that conclude that the presence of cold protons has no impact on the magnetic reconnection rate (Dargent et al., 2017, 2020; Divin et al., 2016; Tenfjord et al., 2019), except when mass loading the system (Dargent et al., 2020) or changing the plasma β (Zaitsev et al., 2021).

In Figure 2a, we can see the relative kinetic energy gains of ions (i) and electrons (e), with $E'_{k,s} = E_{k,s}/|E_m|$ and $E'_{u,s} = E_{u,s}/|E_m|$. By construction, $\sum_s \left(E'_{k,s} + E'_{u,s}\right) = 1$, as all the magnetic energy loss ($E_m < 0$) is converted into particle energy gains ($E_{u/k} > 0$). The results at the early times $\left(t < 30\ \omega_{ci}^{-1}\right)$ are not relevant for our reconnection study, as magnetic reconnection is not fully developed and the area $\mathcal{A}$ hosts several other dynamics (current layer, early reconnection shock, etc.). Figure 2a tells us how the magnetic energy is converted into different forms of kinetic energy for the different particle populations. For these plots, we do not discriminate between hot and cold ions and look at all ions together. We first observe that the curves are very similar for simulations 1 and 2, meaning that the energy partition between magnetic field and electron and ion population as a whole is not significantly impacted by the splitting of ions into several different populations. For $t > 30\ \omega_{ci}^{-1}$, the curves are roughly

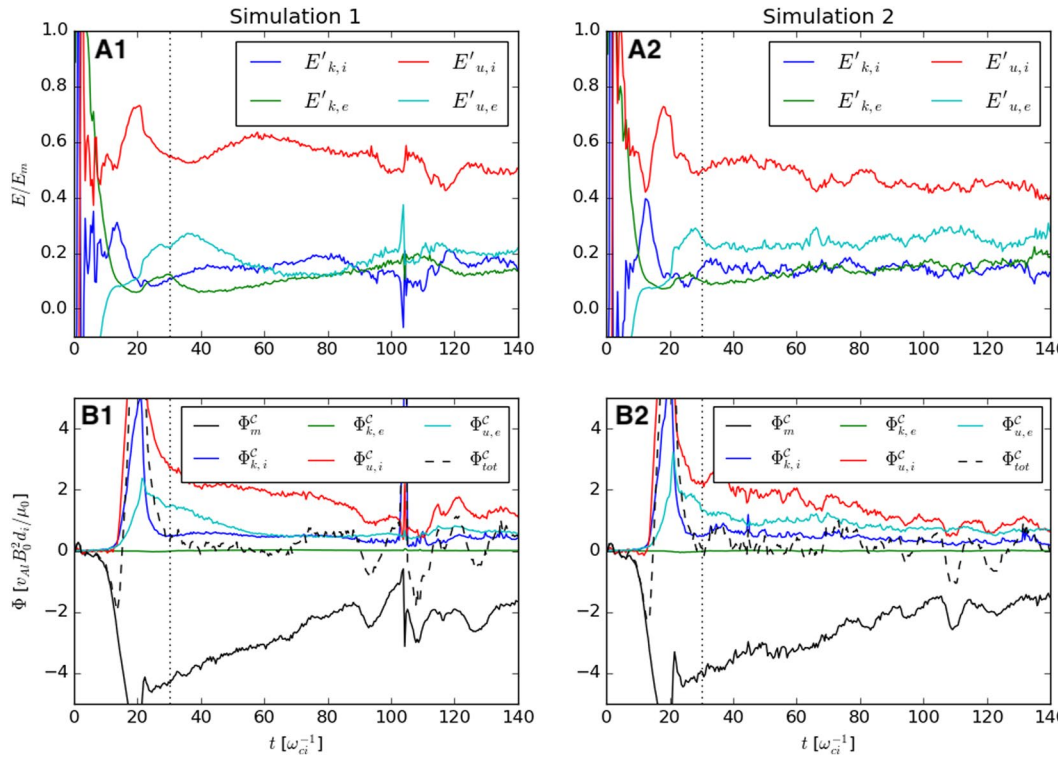

Figure 2. Panel (a1 and a2) relative energy gain of each kinetic source over the area $\mathcal{A}$ for simulation 1 and 2, respectively. Panel (b1 and b2) energy density fluxes through the contour $\mathcal{C}$ for simulation 1 and 2, respectively. $\Phi^{\mathcal{C}}_{tot}$ is the sum of all the other component.

constant, with the exception of $t \sim 105$ in simulation 1, due to the X point shift. The gains mainly go to the heating of ions (54% and 47% of the magnetic energy in average in simulation 1 and 2, respectively, for $t \in [30, 140]\ \omega_{ci}^{-1}$, red curves). The rest is divided between the electron thermal energy gains (19% and 24%, light blue curves), ion kinetic energy gains (15% and 14%, blue curves) and electron kinetic energy gains (12% and 14%, green curves). These results are summarized in Figures 3b and 3c. We see that most of the energy from magnetic reconnection goes into ions and especially into ion heating (Aunai et al., 2011; Eastwood et al., 2013; Haggerty et al., 2015; Shu et al., 2021; Yamada et al., 2014) We observe some differences between the two simulations, which will be further commented upon Section 3.3. In Figure 2b, we see the energy fluxes $\Phi^{\mathcal{C}}_i$, with $i \equiv m, k_s$ or u_s, through the contour $\mathcal{C}$ for both simulations, that is, both the inflowing and outflowing fluxes. As expected, more magnetic energy flows in than out $\left(\Phi^{\mathcal{C}}_m < 0\right)$, while it is the opposite for the other fluxes. We also see on Figure 2b that $\Phi^{\mathcal{C}}_{tot} = \sum_i \Phi^{\mathcal{C}}_i$, is non-zero most of the time. Given that $\sum_i E_i = 0$, $\Phi^{\mathcal{C}}_{tot} = 0$ means either that we are at steady state or that the time derivative terms are balancing each other. We observe the same relative importance of each component for both plots. The decrease in time of the inflowing magnetic flux (i.e., the free magnetic energy density, black curve) is observable on Figure 2b1, correlated with the decrease of the outflowing flux for all the other components. This is the consequence of the slow decrease in time of the reservoir of plasma to reconnect, as the total plasma in the box is constant. The consequence is a slow decrease of both density and magnetic field that reduces the magnetic flux without much impact on magnetic reconnection.

3.3. Relative Energy Transfer to Cold and Hot Ions

After comparing the two simulations with and without cold ions, we are now comparing the energy transfer to the ion populations in simulation 2. In Figure 3a, we plotted the relative kinetic energy gains of each ion populations ions (ions *il* from the initial Harris current layer, hot ions *ih* and cold ions *ic*), with $E'_{k,s} = E_{k,s}/|E_m|$ and $E'_{u,s} = E_{u,s}/|E_m|$. We first see that ion layer's curves quickly go to 0, which proves that the ions present in the initial current layer are quickly pushed away into the exhausts of magnetic reconnection. Once skipping the early times $\left(t > 30\ \omega_{ci}^{-1}\right)$, we can consider that only the inflowing plasma remains. This is why, in Figure 3c, we

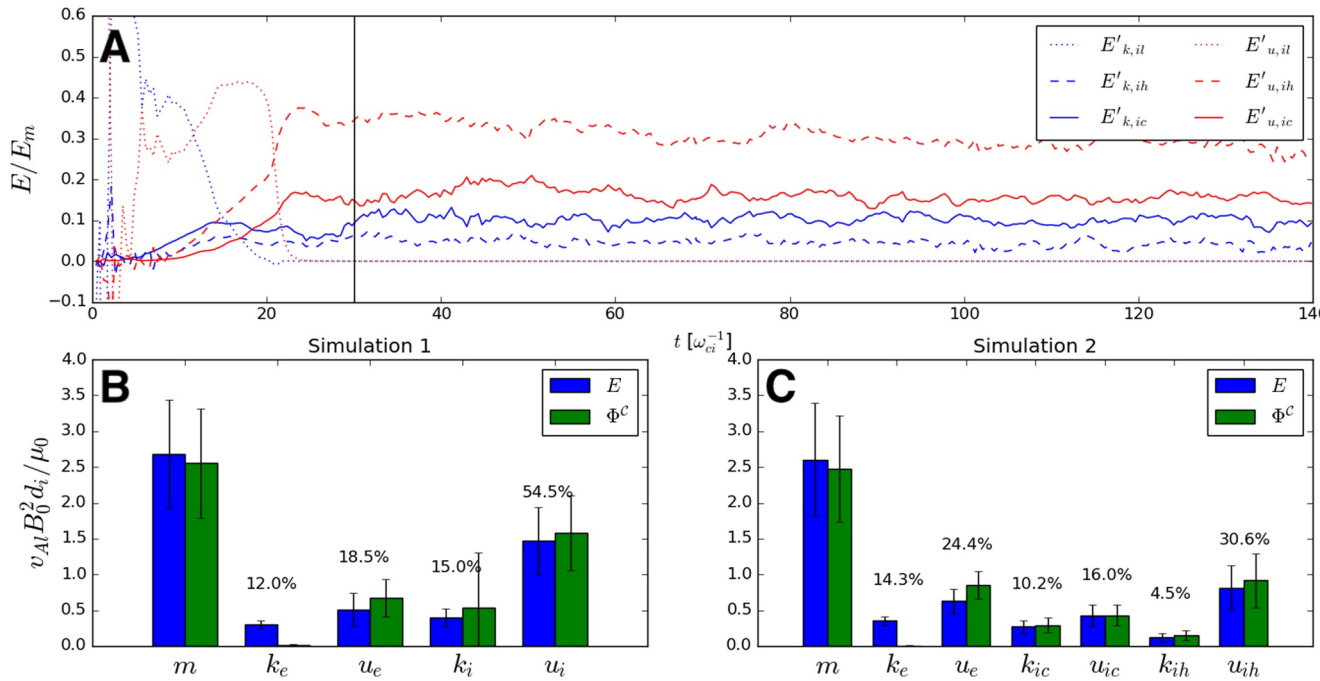

Figure 3. Panel (a) relative energy gain of each kinetic source for each ion population over the area $\mathcal{A}$ in simulation 2. The black line is drawn at $t = 30\ \omega_{ci}^{-1}$. Panel (b) Energy gain E over the area $\mathcal{A}$ and energy density fluxes Φ^C through the contour C averaged over $t \in [30, 140]$ for each source of energy in simulation 1. Standard deviation are plotted using error bar. Above the bars are the percentages of magnetic energy transferred to each term, that is, $E' = E/|E_m|$. Panel (c) Same as panel (b), but in simulation 2.

didn't plot the values for Harris layer's ions (*il*). In Figures 3b and 3c, we averaged the values of E_j and Φ_j^C over $t \in [30, 140]\ \omega_{ci}^{-1}$, for $j \in [m, k_e, u_e, k_i, u_i]$ (simulation 1) and $j \in [m, k_e, u_e, k_{ic}, u_{ic}, k_{ih}, u_{ih}]$ (simulation 2), respectively. We also provide the energy partition, that is, $E' = E_j/|E_m|$, above the bars for sources that gain energy. In these histograms, we first observe that the differences between the averaged E_j and Φ_j^C are small (smaller that the standard deviation), confirming that despite not reaching a steady state, temporal variations are still small enough to allow to draw meaningful conclusions from our analysis. The first simulation shows larger standard deviation, which are mainly due to the plasmoid-induced variation of the curve observed around $t = 105\ \omega_{ci}^{-1}$ (see Figure 2). The only term whose difference between E_j and Φ_j^C is larger than the standard deviation is the electron bulk kinetic energy. This feature, already observed in previous works (Shu et al., 2021), is further developed in Section 4.

When looking at hot and cold ions in Figure 3c, we notice that the majority of converted energy goes into the hot ion thermal energy (31% in Figure 3c, vs. 16% for cold ions), even larger than the electron thermal energy (24%), despite having only half the density of the electrons. On the contrary, when looking at the bulk kinetic energy gains, cold ions get more energy than hot ions (10% vs. 4%). By summing the curves for kinetic and thermal energy gains, we get that 35% of the energy goes to hot ions, 26% to the cold ions and 39% to the electrons. Therefore, the energy transfer per particle ($n_{ic} = n_{ih} = n_e/2$) from magnetic reconnection benefits mainly the most energetic ions, then the low energy ions and finally the electrons. Note that in simulation 2, once normalized by density, we see that the energy transfer is more efficient toward ion populations than toward electrons.

4. Discussion

This study sheds new light on the distribution of the energy gain between hotter and colder ions, in the (quite common) cases when the ion distribution is composed of different populations with different temperature. We focus in particular on the case of symmetric magnetic reconnection. Regarding total kinetic energy gain (kinetic + thermal), the hot ions gain more energy than cold ions. In both cases, most of the energy goes to thermal rather than kinetic energy gain. But the proportion of energy that goes to the thermal (resp. bulk) kinetic energy is quite different for both populations: while 87% of the hot ion energy gain is thermal kinetic, this is only the case of 61% for the cold ions. If we consider all the ions, 76% of the energy gain is thermal kinetic. The

major implication of this result is that, for the cases we studied, the particles in the tail of the velocity distribution function gain more energy than the ones in the core of the distribution. This also means that the entropy rises significantly faster for the hotter ion population compared to the cold population. This open lot of possibilities for the studies of non-Maxwellian distributed plasmas, such as with κ-distributions. Now, these results open two questions: why do hot ions gain more energy, and why is the ratio of bulk to thermal energy gain different for the two ion populations?

To answer the first question, it is interesting to look at the source terms of total kinetic energy, that is, $S_{tot,s} = S_{k_s} + S_{u_s} = \mathbf{J}_s \cdot \mathbf{E}$. In principle, hot and cold ions have the same density and drift velocity in the inflowing plasma, and therefore the same current density. However, they decouple in their respective demagnetization region, and, due to the difference in temperature, the hot ion demagnetization region is larger than the cold ion one. Therefore, the charge separations (and associated current density) related to demagnetization covers a larger area for hot ions with respect to colder ions and the energy source term $S_{tot,h}$ is in average positive on a larger surface. Of course, several factors mitigates the efficiency of the energy transfer. First, in the cold ion demagnetization region, $S_{tot,c} > S_{tot,h}$ due to a higher density of cold ions. Second, the amplitude to the electric field is not constant through the diffusion region and tends to be weaker on the edges (where only hot ions are demagnetized) compared to the center. Those two reasons make the cold ion energy conversion more efficient in the cold ion diffusion region, but they are not enough to compensate the fact that the hot ion diffusion region is approximately twice larger.

Looking at the source terms, we can also understand why, in proportion, hot ions get more thermal energy than cold ions. The thermal kinetic energy source term S_{u_s} depends linearly on pressure, and therefore on temperature. Considering that the density and velocity of each ion population remains roughly similar everywhere, the higher value of S_{u_s} relatively to S_{k_s} for hot ions is due to their higher temperature.

Regarding the comparison between the simulations, we observed no important differences between the energy budgets. It appears that electrons gains a little more energy in average in the simulation with cold ions (see Figures 3b and 3c), but the averaged energy gain difference $\Delta E_e = \langle E_{e,tot}^{Sim\ 2} - E_{e,tot}^{Sim\ 1} \rangle \approx 0.17$ between the two simulations is smaller than the standard deviation of $E_{e,tot}$ in both simulations ($\sigma\left(E_{e,tot}^{Sim\ 1}\right) \approx 0.25$ and $\sigma\left(E_{e,tot}^{Sim\ 2}\right) \approx 0.21$). This is also true for ions, with $\Delta E_i \approx -0.25$ for $\sigma\left(E_{i,tot}^{Sim\ 1}\right) \approx 0.57$ and $\sigma\left(E_{i,tot}^{Sim\ 2}\right) \approx 0.59$. Thus, the difference in the energy partition doesn't seem significant enough. Previous studies showed that for identical macroscopic parameters, the presence of cold ions has no impact on the reconnection rate (Dargent et al., 2017, 2020; Divin et al., 2016). With this work, we addressed the still open question of the impact of cold ion on the global magnetic reconnection energy budget: the energy budget is also unaffected by cold ions, as long as the global parameters are unchanged. And the main recipient of the energy transfer is by far the ion thermal energy density (Aunai et al., 2011; Shu et al., 2021).

Finally, we remark on the difference between $\Phi_{k,e}^C$ and $E_{k,e}$ in Figure 2, for both the simulations without and with cold ions: $E_{k,e}$ is quite larger than $\Phi_{k,e}^C$. The two terms are not expected to be equal in the absence of steady-state, and in fact a significant difference between $\Phi_{k,e}^C$ and $E_{k,e}$ has already been observed in other works (Shu et al., 2021), with a negligible $\Phi_{k,e}^C$ being consistent with observations (Eastwood et al., 2013). In our case, at least part of the difference between the two terms seems to be due to the numerical resolution we use in our simulation. Since we are using a semi-implicit code (hence, we are not forced to solve electron-scale processes out of stability considerations), we have decided to under-resolve electron scales, $dx \approx 0.1 d_i = 1.6 d_e$, in order to make large-scale, high-mass ratio simulations computationally affordable. This is routinely done in cases where the focus is on ion-scale processes (Lapenta et al., 2017). In such cases, it is expected that processes not fully resolved (here, electron-scale processes) are simulated qualitatively rather than quantitatively, see for example, the discussion in Innocenti et al. (2015). A test simulation was performed based on simulation 1 with higher resolution (but for a shorter time, out of computational cost considerations): the $E_{k,e}$ term reduces, without significantly affecting the other values.

5. Conclusions

We showed that for identical macroscopic parameters, the energy partition in magnetic reconnection does not depend significantly on the velocity distribution function (in our case, Maxwellian or double Maxwellian) of the inflowing plasma. Taking advantage of the discrimination we operated between hot and cold ions in the

double-Maxwellian plasma simulation, we show that, for identical density, the hot ions population gains more energy than the cold ion population. We conclude that energy transfer from magnetic to kinetic energy in the context of magnetic reconnection is more efficient for more energetic particles, that is, the tail particles get more energy than the core particles of the plasma distribution. Finally, we also show that the distribution of kinetic energy between bulk and thermal energy density depends directly on the temperature of the inflowing plasma: the hotter the plasma, the higher the thermal energy gain.

The conclusions of this paper open perspectives for the whole domain of non-Maxwellian distribution plasmas. A mostly unchanged global energy budget for magnetic reconnection means that most of the results obtained for Maxwellian plasma can be applied to non-Maxwellian plasma. The fact, however, that the shape of the ion distribution function changes at the end of the simulation as a result of different rates of energy transfer between cold and hot ions may affect secondary processes, not address in this work. Furthermore, the results obtained in this paper are tied to heating and acceleration processes occurring in the diffusion region of magnetic reconnection. Future work is required to understand if this fundamental new results can be extended to other heating and acceleration processes.

Data Availability Statement

The simulation results are generated from ECsim simulation model, as described in Section 2. The simulation data for the figures in the study can be downloaded from https://doi.org/10.5281/zenodo.7639110.

Acknowledgments
JD and MEI acknowledge support from the German Science Foundation DFG within the Collaborative Research Center SFB1491. We also gratefully acknowledge the Gauss Centre for Supercomputing e.V. (www.gauss-centre.eu) for funding this project by providing computing time on the GCS Supercomputer SuperMUC-NG at Leibniz Supercomputing Centre (www.lrz.de). This work used the DiRAC Extreme Scaling service at the University of Edinburgh, operated by the Edinburgh Parallel Computing Centre on behalf of the STFC DiRAC HPC Facility (www.dirac.ac.uk). This equipment was funded by BEIS capital funding via STFC capital Grant ST/R00238X/1 and STFC DiRAC Operations Grant ST/R001006/1. DiRAC is part of the National e-Infrastructure. JD and ME also thank the help of Pr. Giovanni Lapenta for his help with the ECsim code. STR acknowledges support of MCIN/AEI/PRTR 10.13039/501100011033 (Grants PID2020-112805GA-I00 and TED2021-129357A-I00) and Seneca Agency from Region of Murcia (Grant 21910/PI/22). AD was supported by DAAD Dmitrij Mendeleev-Programm, 2021 (N. 57558835).

References

André, M., & Cully, C. M. (2012). Low-energy ions: A previously hidden solar system particle population. *Geophysical Research Letters*, *39*(3), n/a. https://doi.org/10.1029/2011GL050242

Angelopoulos, V., McFadden, J. P., Larson, D., Carlson, C. W., Mende, S. B., Frey, H., et al. (2008). Tail reconnection triggering substorm onset. *Science*, *321*(5891), 931–935. https://doi.org/10.1126/science.1160495

Aunai, N., Belmont, G., & Smets, R. (2011). Energy budgets in collisionless magnetic reconnection: Ion heating and bulk acceleration. *Physics of Plasmas*, *18*(12), 122901. https://doi.org/10.1063/1.3664320

Birn, J., & Hesse, M. (2005). Energy release and conversion by reconnection in the magnetotail. *Annales Geophysicae*, *23*(10), 3365–3373. https://doi.org/10.5194/angeo-23-3365-2005

Birn, J., & Hesse, M. (2010). Energy release and transfer in guide field reconnection. *Physics of Plasmas*, *17*(1), 012109. https://doi.org/10.1063/1.3299388

Dandouras, I. (2013). Detection of a plasmaspheric wind in the Earth's magnetosphere by the Cluster spacecraft. *Annales Geophysicae*, *31*(7), 1143–1153. https://doi.org/10.5194/angeo-31-1143-2013

Dargent, J., Aunai, N., Belmont, G., Dorville, N., Lavraud, B., & Hesse, M. (2016). Full particle-in-cell simulations of kinetic equilibria and the role of the initial current sheet on steady asymmetric magnetic reconnection. *Journal of Plasma Physics*, *82*(3), 905820305. https://doi.org/10.1017/S002237781600057X

Dargent, J., Aunai, N., Lavraud, B., Toledo-Redondo, S., & Califano, F. (2020). Simulation of plasmaspheric plume impact on dayside magnetic reconnection. *Geophysical Research Letters*, *47*(4), e2019GL086546. https://doi.org/10.1029/2019GL086546

Dargent, J., Aunai, N., Lavraud, B., Toledo-Redondo, S., Shay, M. A., Cassak, P. A., & Malakit, K. (2017). Kinetic simulation of asymmetric magnetic reconnection with cold ions. *Journal of Geophysical Research: Space Physics*, *122*(5), 5290–5306. https://doi.org/10.1002/2016JA023831

Divin, A., Khotyaintsev, Y. V., Vaivads, A., André, M., Toledo-Redondo, S., Markidis, S., & Lapenta, G. (2016). Three-scale structure of diffusion region in the presence of cold ions. *Journal of Geophysical Research: Space Physics*, *121*(12), 12001–12013. https://doi.org/10.1002/2016JA023606

Eastwood, J. P., Phan, T. D., Drake, J. F., Shay, M. A., Borg, A. L., Lavraud, B., & Taylor, M. G. G. T. (2013). Energy partition in magnetic reconnection in Earth's magnetotail. *Physical Review Letters*, *110*(22), 225001. https://doi.org/10.1103/PhysRevLett.110.225001

Fuselier, S. A., Burch, J. L., Cassak, P. A., Goldstein, J., Gomez, R. G., Goodrich, K., et al. (2016). Magnetospheric ion influence on magnetic reconnection at the duskside magnetopause. *Geophysical Research Letters*, *43*(4), 1435–1442. https://doi.org/10.1002/2015GL067358

Gonzalez-Herrero, D., Micera, A., Boella, E., Park, J., & Lapenta, G. (2019). ECsim-CYL: Energy conserving semi-implicit particle in cell simulation in axially symmetric cylindrical coordinates. *Computer Physics Communications*, *236*, 153–163. https://doi.org/10.1016/j.cpc.2018.10.026

Gosling, J., Birn, J., & Hesse, M. (1995). Three-dimensional magnetic reconnection and the magnetic topology of coronal mass ejection events. *Geophysical Research Letters*, *22*(8), 869–872. https://doi.org/10.1029/95gl00270

Haggerty, C., Shay, M., Drake, J., Phan, T., & McHugh, C. (2015). The competition of electron and ion heating during magnetic reconnection. *Geophysical Research Letters*, *42*(22), 9657–9665. https://doi.org/10.1002/2015gl065961

Innocenti, M. E., Beck, A., Ponweiser, T., Markidis, S., & Lapenta, G. (2015). Introduction of temporal sub-stepping in the multi-level multi-domain semi-implicit particle-in-cell code Parsek2D-MLMD. *Computer Physics Communications*, *189*, 47–59. https://doi.org/10.1016/j.cpc.2014.12.004

Lapenta, G., Gonzalez-Herrero, D., & Boella, E. (2017). Multiple-scale kinetic simulations with the energy conserving semi-implicit particle in cell method. *Journal of Plasma Physics*, *83*(2), 705830205. https://doi.org/10.1017/S0022377817000137

Micera, A., Zhukov, A., López, R., Boella, E., Tenerani, A., Velli, M., et al. (2021). On the role of solar wind expansion as a source of whistler waves: Scattering of suprathermal electrons and heat flux regulation in the inner heliosphere. *The Astrophysical Journal*, *919*(1), 42. https://doi.org/10.3847/1538-4357/ac1067

Pilipp, W., Miggenrieder, H., Montgomery, M., Mühlhäuser, K.-H., Rosenbauer, H., & Schwenn, R. (1987). Characteristics of electron velocity distribution functions in the solar wind derived from the helios plasma experiment. *Journal of Geophysical Research*, *92*(A2), 1075–1092. https://doi.org/10.1029/ja092ia02p01075

Pritchett, P. L. (2008). Collisionless magnetic reconnection in an asymmetric current sheet. *Journal of Geophysical Research*, *113*(A6), A06210. https://doi.org/10.1029/2007JA012930

Shay, M. A., Drake, J. F., Rogers, B. N., & Denton, R. E. (2001). Alfvénic collisionless magnetic reconnection and the hall term. *Journal of Geophysical Research*, *106*(A3), 3759–3772. https://doi.org/10.1029/1999JA001007

Shibata, K. C., Masuda, S., Shimojo, M., Hara, H., Yokoyama, T., Tsuneta, S., et al. (1995). Hot-plasma ejections associated with compact-loop solar flares. *The Astrophysical Journal*, *451*(2), L83. https://doi.org/10.1086/309688

Shu, Y., Lu, S., Lu, Q., Ding, W., & Wang, S. (2021). Energy budgets from collisionless magnetic reconnection site to reconnection front. *Journal of Geophysical Research: Space Physics*, *126*(10), e2021JA029712. https://doi.org/10.1029/2021JA029712

Spinnangr, S. F., Hesse, M., Tenfjord, P., Norgren, C., Kolstø, H. M., Kwagala, N. K., & Jørgensen, T. M. (2021). The micro-macro coupling of mass-loading in symmetric magnetic reconnection with cold ions. *Geophysical Research Letters*, *48*(13), e2020GL090690. https://doi.org/10.1029/2020GL090690

Tenfjord, P., Hesse, M., Norgren, C., Spinnangr, S. F., & Kolstø, H. (2019). The impact of oxygen on the reconnection rate. *Geophysical Research Letters*, *46*(12), 6195–6203. https://doi.org/10.1029/2019GL082175

Toledo-Redondo, S., André, M., Aunai, N., Chappell, C. R., Dargent, J., Fuselier, S. A., et al. (2021). Impacts of ionospheric ions on magnetic reconnection and Earth's magnetosphere dynamics. *Reviews of Geophysics*, *59*(3), e2020RG000707. https://doi.org/10.1029/2020RG000707

Yamada, M., Yoo, J., Jara-Almonte, J., Ji, H., Kulsrud, R. M., & Myers, C. E. (2014). Conversion of magnetic energy in the magnetic reconnection layer of a laboratory plasma. *Nature Communications*, *5*(1), 1–8. https://doi.org/10.1038/ncomms5774

Zaitsev, I., Divin, A., Semenov, V., Kubyshkin, I., Korovinskiy, D., Deca, J., et al. (2021). Cold ion energization at separatrices during magnetic reconnection. *Physics of Plasmas*, *28*(3), 032104. https://doi.org/10.1063/5.0008118